Interaction of Bupropion with Muscle-Type Nicotinic Acetylcholine Receptors in Different Conformational States[†]

Hugo R. Arias,*,[‡] Fernanda Gumilar,[§] Avraham Rosenberg,[‖] Katarzyna M. Targowska-Duda,[⊥] Dominik Feuerbach,[@] Krzysztof Jozwiak,[⊥] Ruin Moaddel,[‖] Irving W. Wainer,[‖] and Cecilia Bouzat[§]

[‡]*Department of Pharmaceutical Sciences, College of Pharmacy, Midwestern University, Glendale, Arizona 85308,* [§]*Instituto de Investigaciones Bioquímicas de Bahía Blanca, Universidad Nacional del Sur, CONICET, Bahía Blanca, Argentina,* [‖]*Gerontology Research Center, National Institute of Aging, National Institutes of Health, Baltimore, Maryland 20892,* [⊥]*Department of Chemistry, Medical University of Lublin, Lublin, Poland, and* [@]*Neuroscience Research, Novartis Institutes for Biomedical Research, Basel, Switzerland*

ABSTRACT: To characterize the binding sites and the mechanisms of inhibition of bupropion on muscle-type nicotinic acetylcholine receptors (AChRs), structural and functional approaches were used. The results established that bupropion (a) inhibits epibatidine-induced Ca^{2+} influx in embryonic muscle AChRs, (b) inhibits adult muscle AChR macroscopic currents in the resting/activatable state with ~100-fold higher potency compared to that in the open state, (c) increases the desensitization rate of adult muscle AChRs from the open state and impairs channel opening from the resting state, (d) inhibits binding of [³H]TCP and [³H]imipramine to the desensitized/carbamylcholine-bound *Torpedo* AChR with higher affinity compared to the resting/α-bungarotoxin-bound AChR, (e) binds to the *Torpedo* AChR in either state mainly by an entropy-driven process, and (f) interacts with a binding domain located between the serine (position 6′) and valine (position 13′) rings, by a network of van der Waals, hydrogen bond, and polar interactions. Collectively, our data indicate that bupropion first binds to the resting AChR, decreasing the probability of ion channel opening. The remnant fraction of open ion channels is subsequently decreased by accelerating the desensitization process. Bupropion interacts with a luminal binding domain shared with PCP that is located between the serine and valine rings, and this interaction is mediated mainly by an entropy-driven process.

Bupropion is an antidepressant that is also being marketed as an aid to smoking cessation (*1*, *2*). The proposed mechanism of action for bupropion is one in which this drug inhibits the catecholamine reuptake in presynaptic neurons, modulating the concentrations of dopamine and norepinephrine in the synaptic cleft. However, the affinity of bupropion for the neurotransmitter transporter is only moderate, and there is not clear-cut evidence explaining the dual antidepressant and antinicotinic modes of action elicited by bupropion.

In addition to the current clinical uses of bupropion, this drug behaves pharmacologically as a noncompetitive

antagonist (NCA)[1] on several nicotinic acetylcholine receptors (AChRs) (*3*, *4*) (reviewed in ref *5*). AChRs define the paradigm of the Cys-loop ligand-gated ion channel superfamily. This genetically linked superfamily includes types A and C γ-aminobutyric acid, type 3 5-hydroxytryptamine (serotonin), and glycine receptors (reviewed in refs (*6*−*9*)). The malfunctioning of these receptors has been considered as the origin of several neurological disorders (reviewed in refs *8* and *10*). For example, the evidence showing a higher rate of smokers in depressed patients than in the general population supports a possible

[1]Abbreviations: NCA, noncompetitive antagonist; AChR, nicotinic acetylcholine receptor; PCP, phencyclidine; [³H]TCP, [*piperidyl*-3,4-³H(*N*)]-*N*-[1-(2-thienyl)cyclohexyl]-3,4-piperidine; CCh, carbamylcholine; ACh, acetylcholine; α-BTx, α-bungarotoxin; RT, room temperature; BS buffer, binding saline buffer [50 mM Tris-HCl, 120 mM NaCl, 5 mM KCl, 2 mM $CaCl_2$, and 1 mM $MgCl_2$ (pH 7.4)]; NCA, noncompetitive antagonist; K_i, inhibition constant; K_d, dissociation constant; K_a, association constant; k_{off}, dissociation rate constant; k_{on}, association rate constant; IC_{50}, ligand concentration that produces 50% inhibition (of binding or of agonist activation); n_H, Hill coefficient; EC_{50}, agonist concentration that produces 50% AChR activation; TCA, tricyclic antidepressants; DMEM, Dulbecco's modified Eagle's medium; FBS, fetal bovine serum; FLIPR, fluorescent imaging plate reader.

role of AChRs in depression mechanisms (reviewed in ref 11). In this regard, it has been reported that hypercholinergic neurotransmission, which is associated with depressed mood states, may be mediated through excessive neuronal AChR activation and that the therapeutic actions of many antidepressants may be mediated in part through inhibition of one or more AChRs (reviewed in ref 12).

Previous studies have shown that tricyclic antidepressants (TCAs) behave as NCAs of both muscle-type (13) and neuronal-type AChRs (14). Their noncompetitive inhibitory mechanisms with different members of the Cys-loop ligand-gated ion channel superfamily have been elucidated (13, 15) (reviewed in ref 5). More recently, the TCA binding site in the desensitized *Torpedo* AChR has been characterized by [^{3}H]-2-azidoimipramine photolabeling and molecular dynamics (16). Nevertheless, the mechanisms of AChR inhibition elicited by bupropion are poorly understood. In this regard, we want to determine the interaction of bupropion with muscle-type AChRs in different conformational states. To this end, we will use binding and functional approaches, including radioligand competition binding assays using well-known NCAs such as [*piperidyl*-3,4-^{3}H(*N*)]-*N*-[1-(2-thienyl)cyclohexyl]-3,4-piperidine ([^{3}H]TCP) and [^{3}H]imipramine, Ca^{2+} influx and macroscopic current recordings, thermodynamic and kinetic measurements using column-immobilized *Torpedo* AChRs, and molecular docking and dynamics studies. These studies will aid in further drug development.

EXPERIMENTAL PROCEDURES

Materials. [*piperidyl*-3,4-^{3}H(*N*)]-*N*-[1-(2-Thienyl)cyclohexyl]-3,4-piperidine ([^{3}H]TCP, 42−45 Ci/mmol) and [^{3}H]imipramine hydrochloride (47.5 Ci/mmol) were obtained from PerkinElmer Life Sciences Products, Inc. (Boston, MA), and stored in ethanol at −20 °C. Carbamylcholine chloride (CCh), suberyldicholine dichloride, acetylcholine chloride (ACh), tetracaine hydrochloride, (±)-epibatidine, (±)-bupropion hydrochloride, sodium cholate, cholesterol, phosphatidylserine, sphingomyelin, phosphatidic acid, pepstatin, leupeptin, aprotinin, calpain I, calpain II, benzamidine, paramethylsulfonylfluoride (PMSF), and polyethyleneimine were purchased from Sigma Chemical Co. (St. Louis, MO). Phencyclidine hydrochloride (PCP) was obtained through the National Institute on Drug Abuse (NIDA, NIH, Baltimore, MD). α-Bungarotoxin (α-BTx) was obtained from Invitrogen Co. (Carlsbad, CA). [1-(Dimethylamino)naphthalene-5-sulfonamido]ethyltrimethylammonium perchlorate (dansyltrimethylamine) was purchased from Pierce Chemical Co. (Rockford, IL). Salts were of analytical grade.

Preparation of AChR Native Membranes. AChR native membranes were prepared from frozen *Torpedo californica* electric organs obtained from Aquatic Research Consultants (San Pedro, CA) by differential and sucrose density gradient centrifugation, as described previously (17). The total amount of AChR membrane protein was determined by using the bicinchoninic acid protein assay (Pierce Chemical Co.). Specific activities of these membrane preparations were determined by the decrease in dansyltrimethylamine (6.6 μM) fluorescence produced by the titration of suberyldicholine into receptor suspensions

(0.3 mg/mL) in the presence of 100 μM PCP and ranged from 1.0 to 1.2 nmol of suberyldicholine binding sites/mg of total protein (0.5−0.6 nmol of AChR/mg of protein). The AChR membrane preparations were stored at −80 °C in 12% sucrose.

Preparation of the Cellular Membrane Affinity Chromatography (CMAC) Column and Chromatographic System. The CMAC-*Torpedo* AChR column was prepared by the immobilization of solubilized *Torpedo* membranes following a previously described protocol (18). *Torpedo* membranes were first homogenized in buffer A [50 mM Tris-HCl buffer (pH 7.4) containing 1 mM pepstatin A, 0.02 mM leupeptin, 1 mM aprotinin, 1 mM calpain I, 1 mM calpain II, 1 mM benzamidine, 2 mM MgCl$_2$, 3 mM CaCl$_2$, 5 mM KCl, and 0.2 mM PMSF] and subsequently solubilized in buffer A containing 2% (w/v) sodium cholate and 1 mL of glycerol, in the presence of 100 nM cholesterol, 60 μM phosphatidylserine, 20 μM sphingomyelin, and 60 μM phosphatidic acid. Then, 200 mg of the Immobilized Artificial Monolayer (IAM) liquid chromatographic stationary phase (12 μm inside diameter, 300 Å pore, Regis Chemical Co.) was suspended in the supernatant, and the mixture was rotated at room temperature (RT) for 1 h. The suspension was dialyzed against 1 L of 50 mM Tris-saline buffer (pH 7.4) containing 5 mM EDTA, 100 mM NaCl, 0.1 mM CaCl$_2$, and 0.1 mM PMSF for 1 day. The suspension was then centrifuged at 700g and 4 °C, and the pellet (*Torpedo*-IAM) was washed three times with 10 mM ammonium acetate buffer (pH 7.4). The stationary phase was packed into a HR 5/2 column (GE Healthcare, Piscataway, NJ) to yield a 150 mm × 5 mm (inside diameter) chromatographic bed, the CMAC-*Torpedo* AChR column. Finally, the CMAC-*Torpedo* AChR column was attached to the chromatographic system Series 1100 liquid chromatography/mass selective detector (Agilent Technologies, Palo Alto, CA) equipped with a vacuum degasser (G 1322 A), a binary pump (1312 A), an autosampler (G1313 A) with a 20 μL injection loop, a mass selective detector (G1946 B) supplied with atmospheric-pressure ionization electrospray, and an online nitrogen generation system (Whatman, Haverhill, MA). The chromatographic system was interfaced with a 250 MHz Kayak XA computer (Hewlett-Packard, Palo Alto, CA) running ChemStation (revision B.10.00, Hewlett-Packard).

A 10 μL sample of 10 μM bupropion was injected onto the CMAC-*Torpedo* AChR column, and bupropion was monitored in the positive ion mode using single-ion monitoring at *m/z* 240.5 [MW + H]$^+$ ion with a capillary voltage of 3000 V, a nebulizer pressure of 35 psi, and a drying gas flow of 11 L/min at 350 °C.

Cells Expressing Different Muscle-Type AChRs. Human embryonic kidney (HEK293) cells were transfected with mouse α1, β1, δ, and ε cDNA subunits using calcium phosphate precipitation at an α1:β1:δ:ε subunit ratio of 2:1:1:1, essentially as previously described (19, 20). For transfections, cells at 40−50% confluence were incubated for 8−12 h at 37 °C with the calcium phosphate precipitate containing the cDNAs in Dulbecco's modified Eagle's medium (DMEM) with 10% (v/v) fetal bovine serum (FBS). A plasmid encoding green fluorescent protein (pGreen lantern) was also included to allow

identification of transfected cells under fluorescence optics. Cells were used for outside-out patch measurements 1 or 2 days after transfection.

The TE671 cell line is a human rhabdomyosarcoma cell line (obtained from American type Culture Collection) that endogenously expresses the human fetal muscle AChR (i.e., $\alpha 1\beta 1\gamma\delta$). TE671 cells were cultured in a 1:1 mixture of DMEM and Ham's F-12 Nutrient Mixture (Seromed, Biochrom, Berlin, Germany), supplemented with 10% (v/v) FBS. The DMEM/Ham's F-12 mixture contains 1.2 g/L $NaHCO_3$, 3.2 g/L sucrose, and stable glutamine, as previously described (21). The cells were incubated at 37 °C, 5% CO_2, and 95% relative humidity. For passaging, the cells were detached from the cell culture flask by being washed with phosphate-buffered saline and brief incubation (3−5 min) with trypsin (0.5 mg/mL) and EDTA (0.2 mg/mL). The cells were passaged every 3 days.

Ca^{2+} Influx Measurements in TE671 Cells. Ca^{2+} influx was assessed as previously described (21). Briefly, 5×10^4 TE671 cells per well were seeded 72 h prior to the experiment on black 96-well plates (Costar) and incubated at 37 °C in a humidified atmosphere (5% CO_2/95% air); 16−24 h before the experiment, the medium was changed to 1% BSA in a HEPES-buffered salt solution (HBSS) [130 mM NaCl, 5.4 mM KCl, 2 mM $CaCl_2$, 0.8 mM $MgSO_4$, 0.9 mM NaH_2PO_4, 25 mM glucose, and 20 mM HEPES (pH 7.4)]. On the day of the experiment, the medium was removed by flicking the plates and replaced with 100 μL of HBSS/1% BSA containing 2 mM Fluo-4 (Molecular Probes, Eugene, OR) in the presence of 2.5 mM probenecid (Sigma, Buchs, Switzerland). The cells were incubated at 37 °C in a humidified atmosphere (5% CO_2/95% air) for 1 h. Plates were flicked to remove excess of Fluo-4, washed twice with a HBSS/1% bovine serum albumin (BSA) mixture, refilled with 100 μL of HBSS containing different concentrations of bupropion, and preincubated for 5 min. Plates were then placed in the cell plate stage of the fluorescent imaging plate reader (FLIPR) (Molecular Devices, Sunnyvale, CA). A baseline consisting of five measurements of 0.4 s each was recorded. Epibatidine (1 μM) was then added from the agonist plate (placed in the agonist plate stage of the FLIPR) to the cell plate using the FLIPR 96-tip pipettor simultaneously with fluorescence recordings for a total length of 3 min. The laser excitation and emission wavelengths were 488 and 510 nm, respectively, at 1 W, with a CCD camera opening of 0.4 s. In parallel experiments, 1 μM epibatidine with different concentrations of bupropion was co-injected by several seconds.

Patch−Clamp Recordings in HEK293 Cells Expressing Mouse Adult Muscle AChRs. For outside-out recordings, the pipet solution contained 140 mM KCl, 5 mM EGTA, 5 mM $MgCl_2$, and 10 mM HEPES (pH 7.3). Extracellular solution (ECS) contained 150 mM NaCl, 5.6 mM KCl, 1.8 mM $CaCl_2$, 5 mM $MgCl_2$, and 10 mM HEPES (pH 7.3). The patch was excised in this configuration and moved into position at outflow of a perfusion system. The perfusion system allows for a rapid (0.1−1 ms) exchange of the solution bathing patch. A series of applications of 300 μM ACh were applied to the patch,

as described previously (13, 22). The duration of the agonist pulse was 200 ms. We recorded the responses following different protocols. For the $+/-$ protocol, the patch was exposed to bath solution containing different concentrations of bupropion for 2 min before the application of the agonist-containing solution. For the $-/+$ protocol, there was a pulse of agonist solution containing bupropion without preincubation. For the $+/+$ protocol, the patch was exposed to bath solution containing different concentrations of bupropion for 2 min before the application of the agonist solution containing bupropion. All currents were referred to those recorded in the same cell in the absence of bupropion ($-/-$ protocol). In these experiments, control currents were also recorded after each protocol to assess recovery of the original peak current.

Macroscopic currents were filtered at 5 kHz, digitized at 20 kHz, and stored on the hard disk. Data analysis was performed using IgorPro (WaveMetrics Inc., Lake Oswego, OR). The ensemble mean current was calculated for 5−10 individual current traces. Mean currents were fitted by a single-exponential function:[4]

$$I_{(t)} = I_0^{(-t/\tau_d)} + I_\infty \qquad (1)$$

where I_0 and I_∞ are the peak and the steady state current values, respectively, and τ_d is the decay time constant that measures the current decay due to desensitization. Current records were aligned with each other at the point where the currents had risen to 50% of its maximum level. Peak currents correspond to the value obtained by extrapolation of the decay current to this point. The ratio between the peak current or the desensitization rate in the presence ($I_{bupropion}$) and absence of the drug (I_{cont}) was plotted as a function of bupropion concentration, and the curve was fitted to the Hill equation:

$$I_{bupropion}/I_{cont} = IC_{50}{}^{n_H}/(IC_{50}{}^{n_H} + [bupropion]^{n_H}) \quad (2)$$

where IC_{50} is the concentration of bupropion that produces 50% inhibition of the peak currents.

Bupropion-Induced Inhibition of [^{3}H]TCP and [^{3}H] Imipramine Binding to Torpedo AChRs in Different Conformational States. We studied the influence of bupropion on maximal binding of either [^{3}H]TCP or [^{3}H] imipramine to the *Torpedo* AChR in the resting/α-bungarotoxin (α-BTx)-bound and desensitized/CCh-bound states. In this regard, AChR native membranes (0.3 μM) were suspended in binding saline (BS) buffer [50 mM Tris-HCl, 120 mM NaCl, 5 mM KCl, 2 mM $CaCl_2$, and 1 mM $MgCl_2$ (pH 7.4)] with 7 nM [^{3}H]TCP or 13 nM [^{3}H] imipramine in the presence of 1 mM CCh (desensitized/CCh-bound state), or with 7 nM [^{3}H]TCP or 44 nM [^{3}H] imipramine in the presence of 1 μM α-BTx (resting/α-BTx-bound state), and preincubated for 30 min at RT. α-Bungarotoxin is a competitive antagonist that maintains the AChR in the resting (closed) state (23). Nonspecific binding was assessed in the presence of 50 μM PCP (desensitized/CCh-bound state experiments) or 100 μM PCP (or alternatively 200 μM tetracaine) (resting/α-BTx-bound state experiments), as described previously (24, 25). The total volume was divided into aliquots, and increasing concentrations of bupropion were added to

each tube and incubated for 2 h at RT. AChR-bound radioligand was then separated from free ligand by a filtration assay using a 48-sample harvester system with GF/B Whatman filters (Brandel Inc., Gaithersburg, MD), previously soaked with 0.5% polyethyleneimine for 30 min. The membrane-containing filters were transferred to scintillation vials with 3 mL of Bio-Safe II (Research Product International Corp., Mount Prospect, IL), and the radioactivity was determined using a Beckman LS6500 scintillation counter (Beckman Coulter, Inc., Fullerton, CA).

The concentration−response data were curve-fitted by nonlinear least-squares analysis using Prism. The corresponding IC_{50} values were calculated using the following equation:

$$\theta = 1/[1 + ([L]/IC_{50})^{n_H}] \qquad (3)$$

where θ is the fractional amount of the radioligand bound in the presence of inhibitor at a concentration [L] compared to the amount of the radioligand bound in the absence of inhibitor (total binding). IC_{50} is the inhibitor concentration at which θ = 0.5 (50% bound), and n_H is the Hill coefficient. The n_H values were summarized in Table 2.

When the fact that the AChR presents one binding site for TCP (25, 26) and imipramine (13, 16) is taken into account, the observed IC_{50} values from the competition experiments described above were transformed into inhibition constant (K_i) values using the Cheng−Prusoff relationship (27):

$$K_i = IC_{50}/(1 + [NCA]/K_d^{NCA}) \qquad (4)$$

where [NCA] is the initial concentration of [³H]TCP or [³H]imipramine and K_d^{NCA} is the dissociation constant for [³H]TCP [0.83 μM in the resting state (25) and 0.25 μM in the desensitized state (26)] and for [³H]imipramine in the desensitized and resting states [0.8 and 3.8 μM, respectively (16)]. In addition, the free energy change (ΔG) of bupropion interacting with the *Torpedo* AChR was determined (reviewed in ref 7):

$$\Delta G = RT \ln K_i \qquad (5)$$

where R is the gas constant (8.314 J mol^{-1} K^{-1}) and T is the temperature in kelvin. The calculated K_i and ΔG values for bupropion are summarized in Table 2.

Determination of the Binding Kinetics for Bupropion Using the CMAC-Torpedo AChR Column. In the nonlinear chromatography approach, concentration-dependent asymmetric chromatographic traces are observed due to slow adsorption and desorption rates. The mathematical approach used in this study to resolve these nonlinear conditions was the Impulse Input Solution (28). The chromatographic data were analyzed using PeakFit version 4.11 for Windows Software (SPSS Inc., Chicago, IL) following a previously reported protocol (29). The details of this approach and its application to the determination of the binding kinetics of noncompetitive inhibitors to neuronal AChRs were described previously (29, 30). Briefly, the resultant peaks were fitted to the Impulse Input Solution model by adjusting four

variables, namely, $a_0−a_3$. The a_2 variable was directly used for the calculation of the dissociation rate constant (k_{off}) according to this equation:

$$k_{off} = 1/(a_2 t_0) \qquad (6)$$

where the dead time of the column, t_0, is determined as the time required for the elution of water. The a_3 value was used to calculate the association constant (K_a) for the formation of the ligand−receptor complex in equilibrium using this relationship:

$$K_a = a_3/[bupropion] \qquad (7)$$

where [bupropion] is the concentration of bupropion. Both K_a and k_{off} values can be used to further calculate the association rate constant, k_{on} ($k_{on} = K_a k_{off}$).

Thermodynamic Parameters of Torpedo AChR−Bupropion Interactions. Chromatographic elutions of bupropion from the CMAC-*Torpedo* AChR column were carried out at the following temperatures: 10, 12, 16, 20, and 25 °C. The elution procedure was conducted using a mobile phase composed of 10 mM ammonium acetate buffer (pH 7.4) and methanol (85:15, v/v) delivered at a flow rate of 0.2 mL/min. For the first set of experiments, the CMAC-*Torpedo* AChR column was equilibrated by passing 125 nM α-BTx to the mobile phase through the column for 1 h. In addition, a new column was treated with a 10 μL injection of 1 mM epibatidine, and the temperature studies were repeated. All studies were conducted in triplicate.

For the temperature dependence studies, van't Hoff plots were constructed according to the following linear regression equation (reviewed in ref 7):

$$\ln K_a = (\Delta S°/R) − (\Delta H°/R)(1/T) \qquad (8)$$

where $\Delta S°$ and $\Delta H°$ are the standard entropy change and standard enthalpy change, respectively. Finally, the free energy change at 293 K (ΔG^{20}) was calculated using the Gibbs−Helmholtz equation (reviewed in ref 7):

$$\Delta G^{20} = \Delta H° − T\Delta S° \qquad (9)$$

Docking and Molecular Dynamics of (R)- and (S)-Bupropion in Muscle-Type AChR Ion Channels. Amino acid sequences in the M2 transmembrane segments of the AChR ion channel are highly conserved between different species and subunits. However, the absolute numbering of amino acid residues varies greatly between subunits; thus, the residues in M2 of AChR subunits are mentioned here using the prime nomenclature (1′−20′), corresponding to residues Met[243]−Glu[262] in the *Torpedo* AChR α-subunit. As binding targets for modeling, we used a structural model of the pore region of AChR based on the cryo-electron microscopy structure of the *Torpedo* AChR determined at ∼4 Å resolution (Protein Data Bank entry 2BG9) (32, 33). A model of the mouse muscle AChR subtype was constructed using the homology/comparative modeling method with the *Torpedo* 2BG9 model used as a template.

Computational simulations were performed using the same protocol as recently reported (16). In the first step,

Table 1: Inhibitory Potencies of Bupropion on Muscle-Type AChRs

receptor type		method	conformational state	IC_{50}^{a} (μM)	n_H
$\alpha 1\beta 1\gamma\delta$	Ca^{2+} influx	5 min preincubation with bupropion followed by activation with epibatidine for several seconds	mix of different states	20.5 ± 3.9	1.14 ± 0.09
		co-injection of epibatidine and bupropion for several seconds	mix of open and desensitized states	10.5 ± 2.1	1.25 ± 0.16
$\alpha 1\beta 1\varepsilon\delta$	patch$-$clamp	co-incubation of ACh and bupropion for 200 ms	open state	40.1 ± 5.1	0.99 ± 0.11
		2 min preincubation with bupropion followed by activation with ACh for 200 ms	resting/activatable state	0.40 ± 0.04	1.90 ± 0.30

[a] IC_{50} is the required concentration of bupropion to produce 50% inhibition of agonist-activated AChRs determined by Ca^{2+} influx (data not shown) and patch$-$clamp (see Figure 1) methods, respectively.

Table 2: Interaction of Bupropion with the *Torpedo* AChR in Different Conformational States Determined by Radioligand Binding Studies

radioligand	desensitized/CCh-bound state			resting/α-BTx-bound state		
	K_i^{a} (μM)	n_H	ΔG^{b} (kJ/mol)	K_i^{a} (μM)	n_H	ΔG^{b} (kJ/mol)
[^{3}H]TCP	2.0 ± 0.1	1.01 ± 0.06	-32.5 ± 0.1	5.1 ± 0.3	1.20 ± 0.08	-30.2 ± 0.1
[^{3}H]imipramine	11.6 ± 1.3	0.81 ± 0.07	-28.2 ± 0.3	21.4 ± 3.4	0.63 ± 0.06	-26.6 ± 0.4

[a] The K_i values were calculated from Figures 2 ([^{3}H]TCP) and 3 ([^{3}H]imipramine) using eq 4. [b] The ΔG values were calculated using eq 5 at the experimental temperature (298 K).

(*R*)- and (*S*)-bupropion molecules were prepared using HyperChem 6.0 (HyperCube Inc., Gainesville, FL). Sketched molecules were optimized using semiempirical method AM1 (Polak$-$Ribiere algorithm to a gradient lower than 0.1 kcal $\mathring{A}^{-1}$ mol^{-1}) and then transferred for the subsequent step of ligand docking. The Molegro Virtual Docker (MVD 2008.2.4.0, Molegro ApS, Aarhus, Denmark) was used for simulations of docking of flexible ligands into the rigid target AChR model. In this step, the complete structures of target receptors were used. The docking space was limited and centered on the middle of the ion channel and extended enough to ensure covering of the whole channel domain for sampling simulations (docking space was defined as a sphere 21 $\mathring{A}$ in diameter). The actual docking simulations were performed using the following settings: number of runs, 100; maximal number of interactions, 10000; and maximal number of poses, 10. The pose representing the lowest value of the scoring function (MolDockScore) for each ligand was selected for further simulations. In the last step, molecular dynamics were performed using Yasara 6.10.18 (Yasara BioSciences, Graz, Austria). Complexes of *Torpedo* or mouse muscle AChR ion channel models with bupropion isomers were edited to provide coordinates for the membrane domain only. For each subunit, M1$-$M4 transmembrane helices and connecting loops were left in the system, and all other parts of the protein were removed. These models were further inserted into periodic boxes (88 $\mathring{A}$ × 88 $\mathring{A}$ × 68 $\mathring{A}$) and solvated with water molecules using the Yasara default algorithm. Although fixing constraints for backbone atoms were assigned, all side chain atoms were left free to move during the simulations. In all further simulations, the AMBER99 force field for both protein and ligand structures was used (Yasara BioSciences) with a 7.86 $\mathring{A}$ cutoff and particle-mesh Ewald long-range function for electrostatic interactions. The initial complexes were preoptimized with the steepest descent method followed by 500 steps of simulated annealing. Finally, the actual 1.0 ns molecular dynamics was performed using the following parameters: temperature, 298 K; multiple time steps, 1 fs for intramolecular and 2 fs for intermolecular forces; PressureControl, waterprobe (0.99 g/mL) ensemble. Snapshots of the simulations were saved every 5 ps.

The trajectories of molecular dynamics simulations were characterized by calculation of the emulated binding energy defined here as the difference between the energy of the complete complex system and a summation of energy of the ligand and the energy of the hydrated protein alone. All these calculations were performed with the same AMBER force field settings.

RESULTS

Bupropion Inhibits Epibatidine-Mediated Ca^{2+} Influx in TE671 Cells. The change in fluorescence in TE671 cells after epibatidine stimulation is caused by an increase in the intracellular level of Ca^{2+}. The major source of Ca^{2+} is the extracellular buffer. Omission of Ca^{2+} from the extracellular solution does not produce the signal elicited by agonist stimulation (*21*). Epibatidine-induced $\alpha 1\beta 1\gamma\delta$ AChR activation is blocked by preincubation ($\sim$5 min) with bupropion with an inhibitory potency (IC_{50}) of 20.5 ± 3.9 μM (Table 1). Although the receptors are initially in the resting/activatable state (*21*) during preincubation with bupropion, the subsequent addition of the agonist will make them open and desensitized, and therefore, the final effects of bupropion will be a combination of the effects at each state. In addition, the co-injection of epibatidine and bupropion produced an IC_{50} of 10.5 ± 2.1 μM (Table 1). This value is identical to that obtained via $^{86}Rb^{+}$ efflux experiments using the same human muscle AChR (*4*). Considering that this protocol is performed in the time regime of seconds, the observed blocking effect will be a combination of the

effects elicited by bupropion on the open and desensitized ion channels. The fact that the n_H values are close to unity (Table 1) indicates that both bupropion blocking processes are conducted in a noncooperative manner. In turn, this suggests that there is only one binding site for bupropion on each conformational state or that there are binding sites with similar affinities.

Bupropion Inhibits Macroscopic AChR Currents from Resting and Open States by Different Mechanisms. To dissect the effects of bupropion on different conformational states, we studied its effects on outside-out patches

rapidly perfused with 300 μM ACh. To determine the state dependence of bupropion action, we used different perfusion protocols (see Experimental Procedures). In control data, the current reaches the peak after 0.1–1 ms and then decays with a time constant (τ_d) of ~15–30 ms due to desensitization (Figure 1). This τ_d corresponds to a desensitization rate of 37 ± 8 s^{-1}, given that at saturating agonist concentrations $1/\tau_d$ is a good estimation of the desensitized rate. When bupropion is present only in the ACh activation solution ($-/+$ protocol), a concentration-dependent increase in the decay rate ($1/\tau_d$) is observed (Figure 1A). At 200 μM
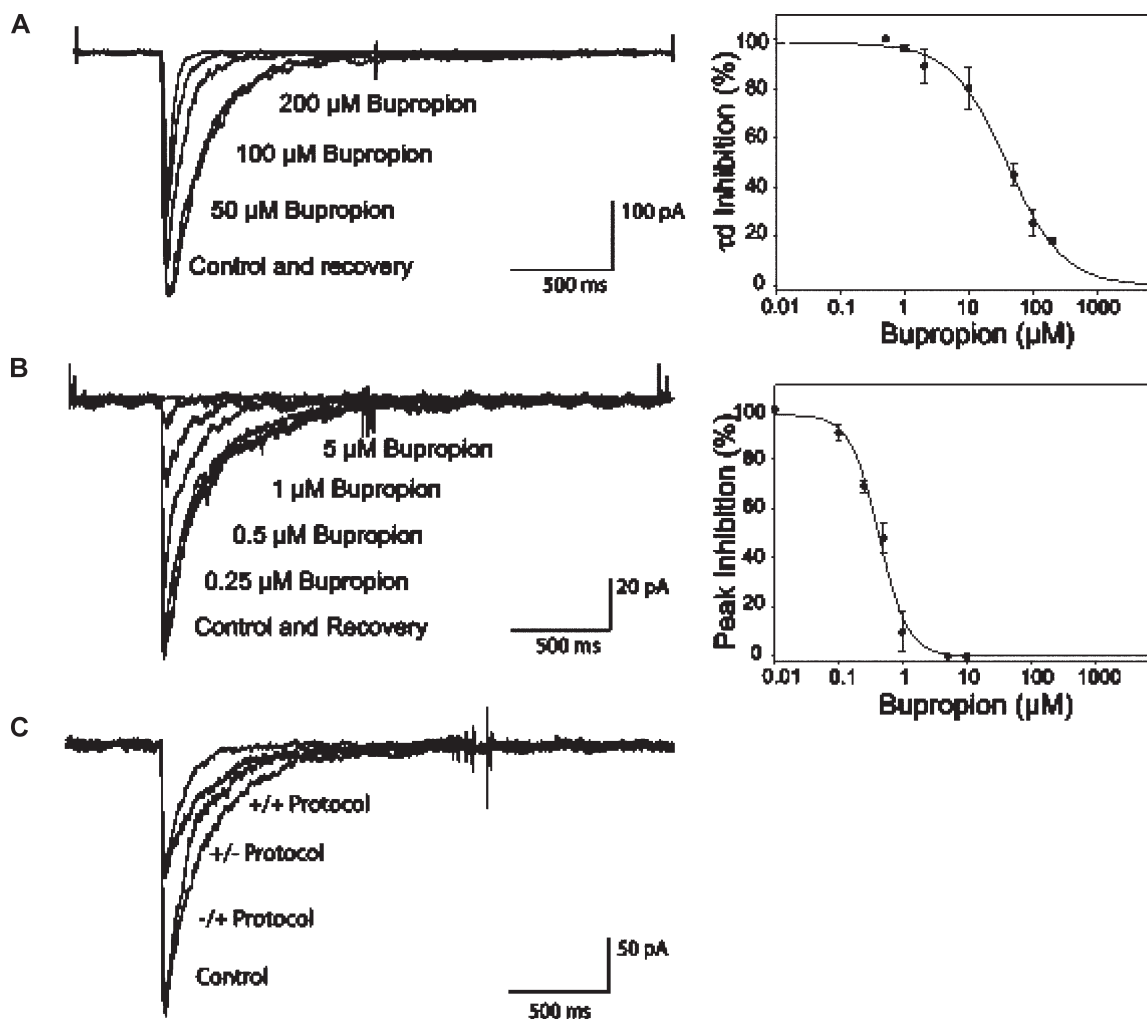

FIGURE 1: Effects of bupropion on agonist-induced macroscopic currents in HEK293 cells expressing mouse $\alpha1\beta1\epsilon\delta$ (adult) AChRs. (A) Bupropion effects from the open state. The left panel shows the ensemble of mean currents obtained from outside-out patches activated in the absence (control) or simultaneous application of ACh and bupropion, without preincubation with bupropion ($-/+$ protocol, open state). Each trace represents the average of four to eight applications of agonist. Curves from right to left correspond to control and recovery, and 50, 100, and 200 μM bupropion. The calculated decay time constants (τ_d) are 25 ms for control and recovery curves and 11.3, 6.3, and 4.5 ms for 50, 100, and 200 μM bupropion, respectively. The membrane potential was -50 mV. The right panel shows the concentration–response curve for the decrease in the decay time constant ($n = 5$). The calculated IC$_{50}$ and n_H values are summarized in Table 1. (B) Effects of bupropion from the resting/activatable state. The left panel shows the effect of the bupropion application $+/-$ protocol (resting/activatable state): 2 min preincubation of bupropion following ACh application. Each trace represents the average of four to eight applications of agonist. Curves from right to left correspond to control and recovery, and 0.25, 0.5, 1, and 5 μM bupropion. The peak current decreases with an increase in bupropion concentration. The membrane potential was -50 mV. The right panel shows the concentration–response curve for the decrease in the peak current on the resting/activatable state. The calculated IC$_{50}$ and n_H values are summarized in Table 1. (C) Effects of bupropion application protocol on macroscopic currents. Superimposed current responses to 300 μM ACh and bupropion concentrations correspond to IC$_{50}$ values for the resting/activatable state [~0.4 μM (see Table 1)] and the open state [~40 μM bupropion (see Table 1)] using different protocols. From right to left curves correspond to control condition ($-/-$ protocol; $\tau_d = 13.4$ ms), simultaneous 300 μM ACh and 40 μM bupropion application without preincubation with bupropion ($-/+$ protocol; $\tau_d = 6.5$ ms; peak current is 99% of the control), ACh application following a 2 min preincubation with 0.4 μM bupropion ($+/-$ protocol; $\tau_d = 13.9$ ms; peak current is 50.4% of the control), and simultaneous 300 μM ACh and 40 μM bupropion application after preincubation with 0.4 μM bupropion ($+/+$ protocol; $\tau_d = 6.3$ ms; peak current is 47% of the control).

bupropion, the decay rate increases to 294 ± 10 s^{-1}. A plot of the normalized decay rate as a function of bupropion concentration yields an IC$_{50}$ value of 40.1 ± 5.1 μM and an n_H of 0.99 ± 0.11 (Table 1). No significant changes in the peak currents are observed under this protocol application. At all bupropion concentrations, decays are well fitted by a single-exponential function. This observation discards a fast open channel block mechanism, since a two-component decay time course should have been observed instead (*34, 35*). However, the observed monoexponential decay might also result from channel block with a slow unblocking rate, as described before for TCAs acting on muscle AChRs (*13*). Distinguishing between slow channel block and increased desensitization is not possible in these experiments.

To determine if bupropion affects AChR activation when acting through the resting/activatable state, we exposed the patch to bupropion for 2 min and then activated the receptors with an ACh solution free of the drug ($+/-$ protocol). Preapplication of the drug decreases the peak current in a dose-dependent manner. No significant changes in the decay rate were observed in the presence of different concentrations of bupropion with respect to control currents. After the drug had been washed out with the bath solution, the peak current can be completely recovered ($95 \pm 2\%$). Thus, the effects of bupropion are very different when it acts on the open state, where it increases the decay rate, or on the resting/ activatable state, where it decreases the peak current. The IC$_{50}$ calculated for the inhibition of the peak current is 0.40 ± 0.04 μM, and the n_H is 1.90 ± 0.30 (Table 1). Thus, the inhibitory potency is much higher when the drug acts from the resting/activatable state than from the open state. The decrease in the peak current produced by bupropion acting at the resting/activatable state may arise from block of resting channels or from an increase in the desensitization of resting channels.

To determine if the effects of bupropion on both states are additive, the patch was continuously exposed to the drug ($+/+$ protocol). For this experiment, we used the drug concentrations corresponding to the IC$_{50}$ values for the actions at each state. Thus, the patch was pre-incubated with 0.4 μM bupropion and then activated with a solution containing 300 μM ACh and 40 μM bupropion. The decrease in the peak current measured in the $+/+$ protocol is quantitatively similar to that measured using the $+/-$ protocol ($48.4 \pm 3.4\%$). Analogously, the decrease in the decay rate determined under the $+/+$ protocol is similar to that achieved under the $-/+$ protocol ($49.5 \pm 2.8\%$). In conclusion, the continuous exposure of the receptor to the drug produces the same inhibition as the sum of the individual effects at the resting/activatable and open states. Full recovery of the peak current and of the decay time constant ($93 \pm 6\%$) is achieved after the drug has been washed, indicating that the inhibition is reversible (Figure 1C).

In conclusion, macroscopic current recordings show that bupropion inhibits AChR by two mechanisms mediated by binding to specific conformational states. More specifically, when bupropion binds to the resting/ activatable state, channel opening is impaired, whereas

when it binds to the open state, the desensitization rate from the open state is increased or, alternatively, slow channel block occurs.

Bupropion-Induced Inhibition of Binding of [^{3}H]TCP or [^{3}H]Imipramine to AChRs in Different Conformational States. We have previously characterized the binding sites for PCP/TCP (*24, 25, 36*) and imipramine (*13, 16*) in *Torpedo* AChRs. Thus, we want to determine the location of the bupropion binding site relative to these NCA loci. To this end, we determined the influence of bupropion on the maximal binding of either [^{3}H]TCP (Figure 2) or [^{3}H]imipramine (Figure 3) to *Torpedo* AChRs in different conformational states. Bupropion inhibits $\sim$100% of the specific binding of [^{3}H]TCP (Figure 2) and [^{3}H]imipramine (Figure 3) to either the desensitized/ CCh-bound or resting/α-BTx-bound state. The obtained K_i values (Table 2) indicate that bupropion binds to the *Torpedo* AChR in either the resting/α-BTx-bound or desensitized/CCh-bound state with practically the same affinity as TCAs (*13, 16*). Comparing the K_i values in different conformational states, we can indicate that
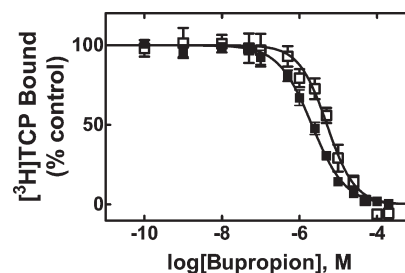

FIGURE 2: Bupropion-induced inhibition of binding of [^{3}H]TCP to *Torpedo* AChRs in the desensitized (CCh-bound) ($\blacksquare$) and resting (α-BTx-bound) ($\square$) states. AChR-rich membranes (0.3 μM) were equilibrated (2 h) with 7 nM [^{3}H]TCP, 1 mM CCh ($\blacksquare$) or 1 μM α-BTx ($\square$), and increasing concentrations of bupropion (i.e., from 1 nM to 200 μM). Nonspecific binding was assessed in the presence of 50 ($\blacksquare$) or 100 μM PCP ($\square$). Each plot is the combination of two separated experiments, each one performed in triplicate. From these plots, the IC$_{50}$ and n_H values were obtained by a nonlinear least-squares fit according to eq 3. Subsequently, the K_i values were calculated using eq 4. The calculated K_i and n_H values are summarized in Table 2.
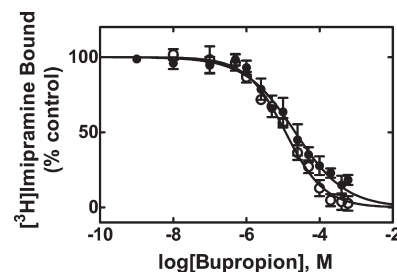

FIGURE 3: Bupropion-induced inhibition of binding of [^{3}H]imipramine to the AChR in the desensitized (CCh-bound) ($\bigcirc$) and resting (α-BTx-bound) ($\bullet$) states. AChR-rich membranes (0.3 μM) were equilibrated (2 h) with 13 nM [^{3}H]imipramine and 1 mM CCh ($\bigcirc$) or with 44 nM [^{3}H]imipramine and 1 μM α-BTx ($\bullet$), and increasing concentrations of bupropion (i.e., from 1 nM to 200 μM). Nonspecific binding was assessed in the presence of 100 μM PCP ($\bigcirc$) or 200 μM tetracaine ($\bullet$). Each plot is a combination of three separated experiments each performed in triplicate. From these plots, the IC$_{50}$ and n_H values were obtained by a nonlinear least-squares fit according to eq 3. Subsequently, the K_i values were calculated using eq 4. The calculated K_i and n_H values are summarized in Table 2.
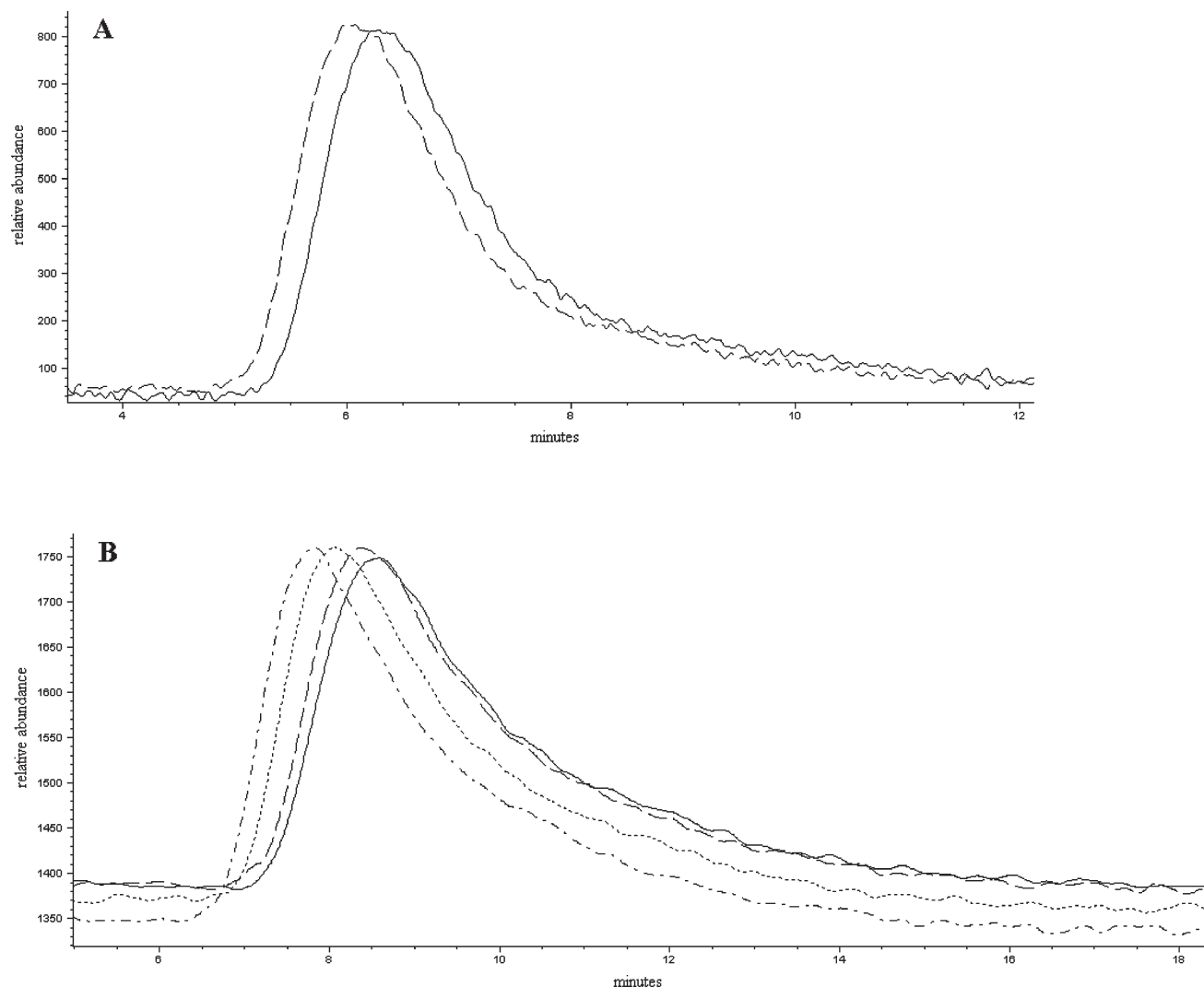
FIGURE 4: Chromatograhic elution of bupropion from the CMAC-*Torpedo* AChR column. (A) Bupropion is eluted from the column with ammonium acetate buffer (10 mM, pH 7.4) and 15% methanol as the mobile phase, at 0.2 mL/min and 20 °C. The dashed line represents the elution of bupropion from the CMAC-*Torpedo* AChR column pretreated with α-BTx (the immobilized AChR is mainly in the resting state), and the solid line represents the elution of bupropion from the CMAC-*Torpedo* nAChR column pretreated with epibatidine (the immobilized AChR is mainly in the desensitized state). (B) Bupropion is eluted from the CMAC-*Torpedo* AChR column pretreated with epibatidine (predominantly desensitized state) at different temperatures (12, 16, 20, and 25 °C from right to left).

bupropion binds to the PCP and TCA binding sites with ~2-fold higher affinity in the desensitized/CCh-bound state compared to that in the resting/α-BTx-bound state. The same binding affinity difference (~1.5-fold) was obtained by using frontal affinity chromatography (data not shown), confirming the radioligand binding results.

The fact that the calculated n_H values are close to unity (Table 2) indicates that bupropion inhibits [³H]TCP and [³H]imipramine binding in a noncooperative manner. These data suggest that bupropion interacts with just one binding site, and that bupropion probably inhibits [³H]TCP and [³H]imipramine binding in a steric fashion. Schild plot analyses of imiprimine-induced [³H]TCP binding inhibition support this mechanism of competition (*37*).

Binding Kinetic Parameters for Bupropion Determined by Column-Immobilized Torpedo AChRs. Figure 4A shows the expected asymmetric traces for bupropion when it is chromatographed on the CMAC-*Torpedo* AChR column. The data were used to determine the

k_{off} and K_a values using eqs 6 and 7, respectively, and thus to further calculate the k_{on} values for bupropion when it binds to the *Torpedo* AChR in different conformational states. These kinetic parameters might help to explain the observed ~2-fold higher affinity of bupropion for the desensitized AChR compared to that for the resting AChR (see Table 2). However, the results indicate that the dissociation rate constant (k_{off}) of bupropion was practically the same when the column was exposed to either epibatidine (the AChR is mainly in the desensitized state) or α-BTx (the AChR is mainly in the resting state) (see Table 3). This is also reflected by similar ΔG values for the resting and desensitized states obtained by kinetic measurements [approximately −31 kJ/mol for both states (see Table 3)], contrary to a small difference in the ΔG values obtained by radioligand binding [−33 and −30 kJ/mol for the desensitized and resting states, respectively (see Table 2)]. In this regard, mechanisms other than ligand kinetics might explain the observed difference in the affinity of bupropion when the receptor is in different conformational states.

Table 3: Kinetic and Thermodynamic Parameters of Binding of Bupropion to *Torpedo* AChRs in Different Conformational States Determined by Nonlinear Chromatography Studies

parameter	α-BTx treated column	epibatidine-treated column
$k_{off}{}^a$ (s^{-1})	0.44 ± 0.01	0.50 ± 0.02
$k_{on}{}^b$ (s^{-1} μM^{-1})	0.16 ± 0.01	0.15 ± 0.02
$K_a{}^c$ (μM^{-1})	0.35 ± 0.03	0.29 ± 0.04
ΔG^{20d} (kJ/mol)	-31.1 ± 0.2	-30.6 ± 0.3

[a] The k_{off} values were empirically determined from Figure 4 according to eq 6. [b] k_{on} values were calculated as $k_{off}K_a$. [c] K_a values were empirically determined from Figure 5 according to eq 7. [d] ΔG values were calculated using eq 5 at the experimental temperature (293 K).

Thermodynamic Parameters for Bupropion Interacting with Torpedo AChRs. In previous studies, an increase in the temperature produced a reduction in the level of chromatographic retention of dextromethorphan and levomethorphan (31). The data could then be analyzed using the van't Hoff plot to calculate the changes in enthalpy (ΔH°) and entropy (ΔS°) associated with the interactions of the ligands with the immobilized AChR. In this paper, nonlinear chromatography was used to calculate the K_a constants to finally construct the van't Hoff plots. In this regard, temperature-dependent changes in bupropion retention on immobilized *Torpedo* AChRs exposed to α-BTx (resting state) were obtained. Since the resulting van't Hoff plot was linear (Figure 5), the thermodynamic parameters ΔH° and ΔS° were calculated from the slopes and intercepts of the van't Hoff plots, respectively, according to eq 8, whereas ΔG^{20} was calculated according to eq 9 (Table 4). Retention of bupropion on immobilized *Torpedo* AChRs exposed to epibatidine (desensitized state) also produced the expected temperature dependence and, thus, a linear van't Hoff plot (Figure 5), allowing the calculation of the respective thermodynamic parameters (Table 4). The linearity of van't Hoff plots indicates an invariant retention mechanism over the temperature range studied (31, 38).

The entropic contributions (i.e., $-T\Delta S^\circ$ values) for the AChR−ligand interactions were calculated using the ΔS° values from Table 4 at 293 K. The results indicate that the entropic contributions are greater (approximately -25 and -26 kJ/mol) than the enthalpic contributions [$\Delta H^\circ \sim -5$ and -6 kJ/mol (see Table 4)] for the resting and desensitized states, respectively. This indicates that the bupropion−AChR interactions in both conformational states were mainly entropy-driven (reviewed in ref 7). In this regard, bupropion may induce local or global conformational changes or solvent reorganization in the binding pocket (reviewed in ref 7). Negative ΔH° values also suggest the existence of attractive forces (e.g., van der Waals, hydrogen bond, and electrostatic interactions) forming the stable complex. The calculated ΔG^{20} values (Table 4) coincide very well with that determined by either radioligand (see Table 2) or chromatographic (see Table 3) experiments. The thermodynamic parameters are similar in both the resting and desensitized states, suggesting that mechanisms other than thermodynamic differences might explain the observed ~2-fold higher affinity of
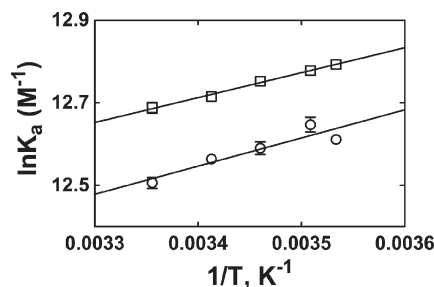

FIGURE 5: van't Hoff plots of bupropion determined by elution from the CMAC-*Torpedo* AChR column at different temperatures (see Figure 4B). Ammonium acetate buffer (10 mM, pH 7.4) and 15% methanol were used as the mobile phase (0.2 mL/min) to elute bupropion from the CMAC-*Torpedo* AChR column at different temperatures (10−25 °C). The column was pretreated with epibatidine (□) (the AChR is mainly in the desensitized state) or with α-BTx (○) (the AChR is mainly in the resting state) before bupropion elution. The plots are the results from three experiments ($n = 3$), where the standard deviation error bars are smaller than the symbol size. The observed r^2 values are 0.995 (□) and 0.998 (○), indicating that the plots are perfectly linear. The ΔH° and ΔS° values were determined using the slope ($\Delta H^\circ = -$slope $\times R$) and y-intercept ($\Delta S^\circ = $ y-intercept $\times R$) values from the plots, according to eq 8, where R is the gas constant (8.314 J K^{-1} mol^{-1}).

Table 4: Thermodynamic Parameters for Binding of Bupropion to the *Torpedo* AChR in Different Conformational States Determined by Nonlinear Chromatography Studies and van't Hoff Analysis

thermodynamic parameter	α-BTx-treated column	epibatidine-treated column
$\Delta H^{\circ a}$ (kJ/mol)	-5.0 ± 0.2	-5.7 ± 1.3
$\Delta S^{\circ a}$ (J mol^{-1} K^{-1})	89 ± 1	85 ± 5
ΔG^{20b} (kJ/mol)	-31.0 ± 0.4	-30.6 ± 1.4

[a] ΔH° and ΔS° were calculated from Figure 5 according to eq 8, [b] ΔG^{20} values were calculated using eq 9.

bupropion for the desensitized state compared to the resting state.

Molecular Dynamics of Bupropion Interacting with Torpedo and Mouse Muscle AChR Ion Channels. During molecular modeling simulations, (R)- and (S)-bupropion isomers were docked to models of *Torpedo* (Figure 6A,B) and mouse muscle AChR ion channels (Figure 6C), respectively. Molegro Virtual Docker generated a series of docking poses and ranked them using energy-based criterion using the embedded scoring function in Mol-DockScore. On the basis of this ranking, the lowest-energy poses of the ligand−receptor complex were selected and are presented in Figure 6A,B (*Torpedo* model) and Figure 6C (mouse muscle model), respectively. The MolDockScore values for best ranked complexes are presented in Table 5. These data serve to compare only the interaction of bupropion isomers with each AChR model (*Torpedo* and muscle mice AChRs, respectively) and are not expected to be considered reliable in absolute terms. In other words, these values cannot be compared to those obtained by other experimental procedures.

Molecular modeling results also indicate that either (R)- or (S)-bupropion in the neutral state interacts within the middle portion of the channel in the cavity formed between valine (position 13′) and serine (position 6′) rings. Interestingly, the same docking site for both isomers in
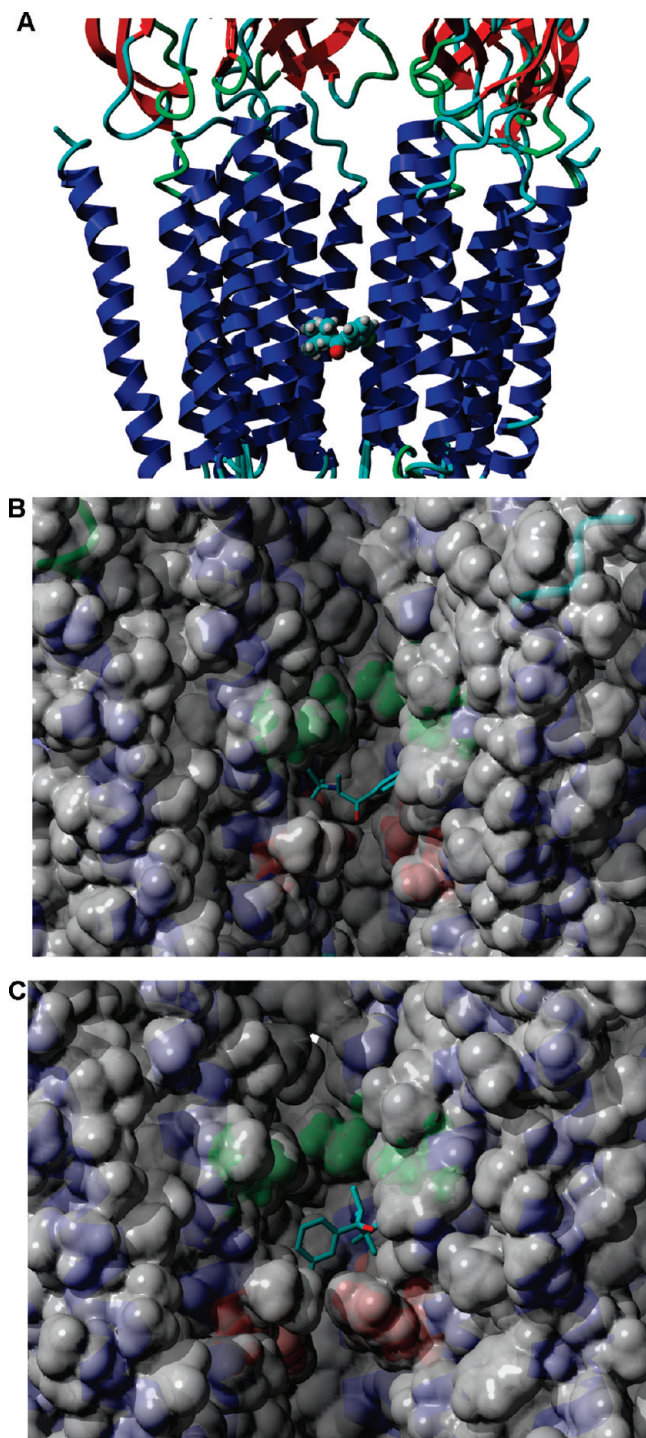
Table 5: MolDockScore Values for the Lowest Energy of the AChR−Bupropion Complex Obtained by Molecular Docking and Average Binding Energies of (*R*)- and (*S*)-Bupropion (in the neutral form) Interacting with *Torpedo* and Mouse Muscle AChR Ion Channels, Respectively, Calculated by Molecular Dynamics

	Torpedo AChR		mouse muscle AChR	
isomer	MolDockScore (kJ/mol)	emulated binding energy[a] (kJ/mol)	MolDockScore (kJ/mol)	emulated binding energy[a] s(kJ/mol)
(*R*)-bupropion	−87.7	−104 ± 10	−97.3	−118 ± 12
(*S*)-bupropion	−87.2	−115 ± 9	−96.7	−113 ± 13

[a] The emulated binding energy was sampled every 5 ps from a total of 1000 ps of molecular dynamics simulation. Standard deviation values for the emulated binding energy represent the fluctuations during molecular dynamics simulations.

channel (*29, 39*). Analyses of the complexes show that the docked molecule interacts only with all five M2 helices, provided by each subunit. Comparison of Molegro scoring function values (see Table 5) suggests that both bupropion enantiomers exhibit lower energies (a difference of approximately −10 kJ/mol) of interaction with the mouse muscle AChR ion channel when compared to the *Torpedo* model.

Best scored complexes obtained by docking were edited and limited to the membrane domain of the receptor and then subjected to molecular dynamics simulations as described in Experimental Procedures. To verify whether the ligand configuration is stable within the binding site, simulations were performed by keeping the backbone of the protein frozen, while the ligand and all side chains were left free to move. Although the simulations lasted for 1.0 ns, the systems reached equilibrium after 0.2−0.25 ns as monitored by the trajectory of total energy (data not shown). During dynamics simulations, the molecules did not significantly change the position compared to the starting pose, indicating that that simulated ligand−receptor complex is stable. In fact, the molecules interacted exclusively with nearby pore-lining residues at overlapping sites between the serine (position 6′) and valine (position 13′) rings, without interacting with the external or intracellular mouths of the ion channel. Table 5 includes the emulated binding energy values averaged during the 1.0 ns trajectory of molecular dynamics for each complex. Although these emulated measurements cannot be considered absolute values, they show that the calculated binding energy values fluctuate significantly during the dynamics simulations, producing standard deviations of ~10% of the averaged value. In this respect, there is no significant difference between the emulated binding energy values for bupropion in the neutral state interacting with either the *Torpedo* AChR or the mouse muscle AChR. This lack of difference between both AChR types was also seen with bupropion in the protonated state. On the basis of these results, we did not pursue additional studies to demonstrate the difference between both isomers on muscle-type AChRs. However, further experiments need to be performed to demonstrate whether this is also true on neuronal-type AChRs such as the α3β4 AChR where bupropion also binds (*4*).

FIGURE 6: Complex formed between (*R*)-bupropion and the *Torpedo* AChR (A and B) and between (*S*)-bupropion and the mouse muscle AChR (C) ion channel obtained by molecular docking. (A) Side view of the lowest-energy complex showing four *Torpedo* subunits rendered in secondary structure mode, with the ligand in the neutral form rendered in element color-coded ball mode. Side views of the *Torpedo* (B) and mouse muscle (C) AChR subunits rendered in semitransparent surface with visible secondary structure and explicit CPK atoms of residues forming the valine (position 13′ in green) and serine (position 6′ in red) rings. The ligand in the neutral form is rendered in stick mode with hydrogen atoms not shown explicitly. In both panels, the δ subunit was removed for the sake of clarity, and the order of remaining subunits is (from left to right) α1, γ, α1, and β1.

the protonated state was found (data not shown). A very similar mode of binding was observed in previous simulations in which bupropion was docked into the α3β4 ion

DISCUSSION

Bupropion clinically acts as an antidepressant, and it is now also marketed as an aid to smoking cessation (*2*). Pharmacologically, bupropion also behaves as a NCA on several AChR types (reviewed in ref *5*). In this regard, this study is an attempt to characterize the interactions of bupropion with different muscle-type AChRs in distinct conformational states and to determine its molecular mechanisms of inhibition. To this end, radioligand competition binding experiments, Ca^{2+} influx and macroscopic current recordings, thermodynamic and kinetic measurements, and molecular docking and dynamics studies were performed.

Molecular Mechanisms of Inhibition Mediated by Bupropion. In a first attempt to determine the effect of bupropion on epibatidine-activated Ca^{2+} influx in TE671 cells, preincubation and co-injection protocols were used. The inhibitory potency of bupropion was in the $10-20$ μM concentration range as was previously determined by $^{86}Rb^+$ efflux experiments using the same cell type (*4*). Since the Ca^{2+} influx approach could not distinguish the effect of bupropion on a particular conformational state, we recorded macroscopic currents of agonist-activated receptors rapidly preincubated (mainly in the resting state) or co-incubated (mainly in the open state) with bupropion (Figure 1).

Macroscopic currents show that the interaction of bupropion with the open state decreases the decay time constant of currents activated by 300 μM ACh. At this ACh concentration, the decay rate equals the rate of desensitization from the double-liganded open state (*40*). Thus, our results reveal that from the open state bupropion increases the desensitization rate. The current decay was adequately fitted using a single-exponential function, which discards the possibility of a fast open channel blockade mechanism. However, the occurrence of slow channel blockade, which has been described for other NCAs (*41*), may result in similar changes in macroscopic currents. If bupropion blocked the AChR and its unblocking process were quite slow, distinguishing between this process and the increase in the desensitization rate would be difficult (*13*).

Macroscopic current recordings also show a decrease in the peak current when bupropion interacts with the resting/activatable channel. Thus, together with the acceleration of the decay rate from the open state, bupropion inhibits the opening of channels by binding to the resting/activatable state. The latter effect might be due to either an increase in the desensitization of the resting/activatable state or a direct blockade of unliganded channels. A similar effect is observed with TCAs (*13*). The potency of inhibition is greater when bupropion acts on the resting/activatable state than on the open state. A similar finding was reported for the inhibition of different Cys-loop receptors by TCAs (*15, 42*).

The two different effects detected for each different conformational state, i.e., reduced peak current and increased decay rate, are additive when the receptor is exposed continuously to the drug. Thus, the mechanism by which bupropion inhibits AChR function is selective for each conformational state.

Characterization of the Bupropion Binding Site. The results from the radioligand competition binding experiments (see Table 2) and frontal chromatographic (data not shown) experiments indicate that bupropion binds with higher affinity to the desensitized/agonist-bound *Torpedo* AChR than to the resting/α-BTx-bound AChR. Unfortunately, neither the kinetic nor the thermodynamic studies could explain the observed state-dependent ligand affinity (see Table 3).

The radioligand competition experiments also indicate that bupropion inhibits the binding of both [^{3}H]imipramine and [^{3}H]TCP (the structural and functional analogue of PCP) to both desensitized/CCh-bound and resting/α-BTx-bound AChRs with n_H values close to unity (Table 2). Hill coefficients close to unity indicate a noncooperative interaction between bupropion and PCP or imipramine, suggesting that bupropion interacts with only one binding site on each AChR conformational state. Although this evidence suggests a steric mode of competition between bupropion and PCP or imipramine, we cannot predict whether the location of the bupropion binding site is the same or distinct in each conformational state.

The location of the PCP binding site depends on the conformational state of the AChR ion channel (reviewed in ref *5*). For instance, photoaffinity labeling studies using [^{3}H]ethidium diazide, which binds with high affinity to the PCP locus, helped to determine the structural components of this site in the desensitized state (*43*). The results indicated that [^{3}H]ethidium diazide mainly labeled residues at and close to the leucine ring (position 9′) from the α1-M2 transmembrane segment. In addition, new photoaffinity labeling results using the hydrophobic probe 3-(trifluoromethyl)-3-(m-[^{125}I]iodophenyl)diazirine suggest that the PCP binding site is located between the threonine (position 2′) and serine (position 6′) rings, closer to the cytoplasmic end of the desensitized ion channel (*44*). Our photoaffinity labeling studies using [^{3}H]-2-azidoimipramine support the idea that TCAs bind to the PCP locus in the desensitized ion channel (*16*). On the other hand, site-directed mutagenesis studies determined that the PCP binding site in the open ion channel includes residues located between the serine (position 6′) and leucine (position 9′) rings (*45*). Finally, we suggested that the PCP binding site in the resting state is located closer to the external mouth than that in the desensitized and open states (*24, 25, 36*). We also speculated that the aromatic tertiary amino group from the PCP (or TCP) molecule might interact with acidic residues (i.e., α1-Glu^{262}) located at position 20′ (e.g., the outer or extracellular ring) (*25, 36*) (reviewed in ref *5*). Considering our previous findings, we suggest that the secondary amino group from the bupropion molecule can also be responsible for the binding to one of the two Glu^{262} residues by charge interactions, when the receptor is in the resting/α-BTx-bound state.

Proposed mechanisms of bupropion binding were additionally studied by molecular modeling. Docking simulations followed by molecular dynamics of (*R*)- and (*S*)-bupropion were performed on two different variants of the AChR membrane domain, *Torpedo* (Figure 6A,B) and mouse muscle (Figure 6C) AChRs. The results from the docking simulations indicate no enantioselective interactions: both enantiomers form ligand−receptor

complexes characterized by similar values of scoring function (Table 5). Although there is no experimental evidence of bupropion enantioselectivity on AChRs, the (2R,3R)-hydroxy bupropion isomer inhibits the muscle-type AChR with 3.7-fold higher potency than the (2S,3S)-hydroxy bupropion isomer (*46*), indicating the possibility of bupropion enantioselectivity. To determine bupropion enantioselectivity in AChRs, bupropion isomers will be used in further functional and binding experiments.

The analysis of the obtained molecular complexes clearly indicates that bupropion in either the neutral (see Figure 6) or protonated form (data not shown) binds to the middle portion of the channel between the serine (position 6′) and valine (position 13′) rings. Exactly the same locus was observed for PCP and imipramine in the *Torpedo* AChR ion channel (*16*). However, a distinction was observed in the α3β4 ion channel: bupropion in the protonated state interacted with the polar region of the intermediate ring (position 1′), whereas the neutral form was positioned between the valine/phenylalanine (position 15′) and serine (position 8′) rings (*29*). The pocket formed by the cleft between the phenyl ring provided by β4-Phe and the isopropyl moiety from α3-Val interacts with the hydrophobic portion of bupropion, whereas hydrogen bonds are formed between polar residues at the serine ring and the polar region of bupropion. Considering this difference, distinct bupropion binding site locations may exist on each AChR ion channel. Nevertheless, we have to take into consideration the fact that the α3β4 AChR ion channel was constructed by homology with the model of the 23-mer peptide imitating the M2 sequence of the *Torpedo* AChR δ subunit (*29*), whereas the current model was based on the cryo-electron microscopy structure of the *Torpedo* AChR determined at ∼4 Å resolution (Protein Data Bank entry 2BG9) (*32, 33*).

The evidence obtained by molecular docking on the *Torpedo* AChR supports the competition experiments (see Table 2), indicating that there is a binding site for antidepressants that overlaps the PCP binding site in the *Torpedo* AChR ion channel. The thermodynamic parameters indicate that bupropion interacts with the *Torpedo* AChR ion channel either in the resting or in the desensitized state mainly by an entropy-driven process (see Table 4). In this regard, bupropion may induce local or global conformational changes or solvent reorganization in the binding pocket. Negative enthalpic values also suggest the existence of attractive forces (e.g., van der Waals, hydrogen bond, and polar interactions) forming the stable complex.

Considering the results described above, we envision a dynamic process in which bupropion binds first to the resting AChR, probably close to the mouth of the ion channel, decreasing the probability of ion channel opening. The remnant fraction of open ion channels is subsequently decreased by accelerating the desensitization process, and less probable by an open channel blocking mechanism. Bupropion inhibits AChR function by interacting with a binding domain shared by tricyclic antidepressants and by PCP that is located between the serine and valine rings. This drug−receptor interaction is mediated mainly by an entropy-driven process.

NOTE ADDED AFTER ASAP PUBLICATION

After this paper was published ASAP April 10, 2009, changes were made to the next-to-last paragraph of the Discussion section; the corrected version was reposted May 7, 2009.

REFERENCES

1. Hurt, R. D., Sachs, D. P., Glover, E. D., Offord, K. P., Johnston J. A., Dale, L. C., Khayrallah, M. A., Schroeder, D. R., Glover, P. N., Sullivan, C. R., Croghan, I. T., and Sullivan, P. M. (1997) A comparison of sustained-release bupropion and placebo for smoking cessation. *N. Engl. J. Med. 337*, 1195–1202.
2. Wonnacott, S., and Barik, J. (2007) Nicotinic ACh Receptors. *TOCRIS Rev. 28*, 1–20.
3. Slemmer, J. E., Martin, B. R., and Damaj, M. I. (2000) Bupropion is a nicotinic antagonist. *J. Pharmacol. Exp. Ther. 295*, 321–327.
4. Fryer, J. D., and Lukas, R. J. (1999) Noncompetitive functional inhibition at diverse, human nicotinic acetylcholine receptor subtypes by bupropion, phencyclidine, and ibogaine. *J. Pharmacol. Exp. Ther. 288*, 88–92.
5. Arias, H. R., Bhumireddy, P., and Bouzat, C. (2006) Molecular mechanisms and binding site locations for noncompetitive antagonists of nicotinic acetylcholine receptors. *Int. J. Biochem. Cell Biol. 38*, 1254–1276.
6. Arias, H. R. ((2006)) Ligand-gated ion channel receptor superfamilies. In *Biological and Biophysical Aspects of Ligand-Gated Ion Channel Receptor Superfamilies* (Arias, H. R., Ed.) pp 1−25, Research Signpost, India.
7. Arias, H. R. ((2001)) Thermodynamics of nicotinic receptor interactions. In *Drug-Receptor Thermodynamics: Introduction and Applications* (Raffa, H. R., Ed.) pp 293−358, John Wiley & Sons, Ltd., New York.
8. Hogg, R. C., Raggenbass, M., and Bertrand, D. (2003) Nicotinic acetylcholine receptors: from structure to brain function. *Rev. Physiol. Biochem. Pharmacol. 147*, 1–46.
9. Lester, H. A., Dibas, M. I., Dahan, D. S., Leite, J. F., and Dougherty, D. A. (2004) Cys-loop receptors: New twists and turns. *Trends Neurosci. 27*, 329–336.
10. Lloyd, G. K., and Williams, M. (2000) Neuronal nicotinic acetylcholine receptors as novel drug targets. *J. Pharmacol. Exp. Ther. 292*, 461–467.
11. Picciotto, M. R., Brunzell, D. H., and Caldarone, B. J. (2002) Effect of nicotine and nicotinic receptors on anxiety and depression. *NeuroReport 13*, 1097–1106.
12. Shytle, R. D., Silver, A. A., Lukas, R. J., Newman, M. B., Sheehan, D. V., and Sanberg, P. R. (2002) Nicotinic receptors as targets for antidepressants. *Mol. Psychiatry 7*, 525–535.
13. Gumilar, F., Arias, H. R., Spitzmaul, G., and Bouzat, C. (2003) Molecular mechanisms of inhibition of nicotinic acetylcholine receptors by tricyclic antidepressants. *Neuropharmacology 45*, 964–976.
14. Rana, B., McMorn, S. O., Reeve, H. L., Wyatt, C. N., Vaughan, P. F., and Peers, C. (1993) Inhibition of neuronal nicotinic acetylcholine receptors by imipramine and desipramine. *Eur. J. Pharmacol. 250*, 247–251.
15. Gumilar, F., and Bouzat, C. (2008) Tricyclic antidepressant inhibit homomeric Cys-loop receptors by acting at different conformational states. *Eur. J. Pharmacol. 584*, 30–39.
16. Sanghvi, M., Hamouda, A. K., Jozwiak, K., Blanton, M. P., Trudell, J. R., and Arias, H. R. (2008) Identifying the binding site(s) for antidepressants on the *Torpedo* nicotinic acetylcholine receptor: [^{3}H]2-Azidoimipramine photolabeling and molecular dynamics studies. *Biochim. Biophys. Acta 1778*, 2690–2699.
17. Pedersen, S. E., Dreyer, E. B., and Cohen, J. B. (1986) Location of ligand-binding sites on the nicotinic acetylcholine receptor α-subunit. *J. Biol. Chem. 261*, 13735–13743.

18. Moaddel, R., Jozwiak, K., Whittington, K., and Wainer, I. W. (2005) Conformational mobility of immobilized $\alpha\beta32,\alpha3\beta4$, $\alpha4\beta2,\alpha4\beta4$ nicotinic acetylcholine receptors. *Anal. Chem. 77*, 895–901.

19. Bouzat, C., Bren, N., and Sine, S. M. (1994) Structural basis of the different gating kinetics of fetal and adult nicotinic acetylcholine receptors. *Neuron 13*, 1395–1402.

20. Bouzat, C., Barrantes, F., and Sine, S. M. (2000) Nicotinic receptor fourth transmembrane domain: Hydrogen bonding by conserved threonine contributes to channel gating kinetics. *J. Gen. Physiol. 115*, 663–672.

21. Michelmore, S., Croskery, K., Nozulak, J., Hoyer, D., Longato, R., Weber, A., Bouhelal, R., and Feuerbach, D. (2002) Study of the calcium dynamics of the human $\alpha4\beta2$, $\alpha3\beta4$ and $\alpha1\beta1\gamma\delta$ nicotinic acetylcholine receptors. *Naunyn-Schmiedeberg's Arch. Pharmacol. 366*, 235–245.

22. Liu, Y., and Dilger, J. P. (1991) Opening rate of acetylcholine receptor channels. *Biophys. J. 60*, 424–432.

23. Moore, M. A., and McCarthy, M. P. (1995) Snake venom toxins, unlike smaller antagonists, appear to stabilize a resting state conformation of the nicotinic acetylcholine receptor. *Biochim. Biophys. Acta 1235*, 336–342.

24. Arias, H. R., McCardy, E. A., Bayer, E. Z., Gallagher, M. J., and Blanton, M. P. (2002) Allosterically linked noncompetitive antagonist binding sites in the resting nicotinic acetylcholine receptor ion channel. *Arch. Biochem. Biophys. 403*, 121–131.

25. Arias, H. R., Trudell, J. R., Bayer, E. Z., Hester, B., McCardy, E. A., and Blanton, M. P. (2003) Noncompetitive antagonist binding sites in the *Torpedo* nicotinic acetylcholine receptor ion channel. Structure-activity relationship studies using adamantane derivatives. *Biochemistry 42*, 7358–7370.

26. Pagán, O. R., Eterović, V. A., Garća, M., Vergne, D., Basilio, C. M., Rodríguez, A. D., and Hann, R. M. (2001) Cembranoid and long-chain alkanol sites on the nicotinic acetylcholine receptor and their allosteric interaction. *Biochemistry 40*, 11121–11130.

27. Cheng, Y., and Prusoff, W. H. (1973) Relationship between the inhibition constant (K_i) and the concentration of inhibitor which causes 50% inhibition (IC_{50}) of an enzymatic reaction. *Biochem. Pharmacol. 22*, 3099–3108.

28. Wade, J. L., Bergold, A. F., and Carr, P. W. (1987) Theoretical description of nonlinear chromatography, with applications to physicochemical measurements in affinity chromatography and implications for preparative-scale separations. *Anal. Chem. 59*, 1286–1295.

29. Jozwiak, K., Ravichandran, S., Collins, J. S., and Wainer, I. W. (2004) Interaction of noncompetitive inhibitors with an immobilized $\alpha3\beta4$ nicotinic acetylcholine receptor investigated by affinity chromatography, quantitative-structure activity relationship analysis, and molecular docking. *J. Med. Chem. 47*, 4008–4021.

30. Moaddel, R., Jozwiak, K., and Wainer, I. W. (2007) Allosteric modifiers of neuronal nicotinic receptors: New methods, new opportunities. *Med. Res. Rev. 27*, 723–753.

31. Jozwiak, K., Hernandez, S., Kellar, K. J., and Wainer, I. W. (2003) The enantioselective interactions of dextromethorphan and levo-methorphan with the $\alpha3\beta4$-nicotinic acetylcholine receptor: Comparison of chromatographic and functional data. *J. Chromatogr., B 797*, 373–379.

32. Unwin, N. (2005) Refined structure of the nicotinic acetylcholine receptor at 4 Å resolution. *J. Mol. Biol. 346*, 967–989.

33. Miyazawa, A., Fujiyoshi, Y., and Unwin, N. (2003) Structure and gating mechanism of the acetylcholine receptor pore. *Nature 423*, 949–955.

34. Dilger, J. P., Boguslavsky, R., Barann, M., Katz, T., and Vidal A. M. (1997) Mechanisms of barbiturate inhibition of acetylcholine receptor channels. *J. Gen. Physiol. 109*, 401–414.

35. Forman, S. A. (1999) A hydrophobic photolabel inhibit nicotinic acetylcholine receptors via open-channel block following a slow step. *Biochemistry 38*, 14559–14564.

36. Arias, H. R., Bhumireddy, P., Spitzmaul, G., Trudell, J. R., and Bouzat, C. (2006) Molecular mechanisms and binding site location for the noncompetitive antagonist crystal violet on nicotinic acetylcholine receptors. *Biochemistry 45*, 2014–2026.

37. Sullivan, C. L., Crundsen, M., and Arias, H. R. ((2008)) Characterization of antidepressant binding sites on the nicotinic acetylcholine receptor. 2008 ACCP Spring Practice and Research Forum, Phoenix, AZ, April 5−9.

38. Jozwiak, K., Haginaka, J., Moaddel, R., and Wainer, I. W. (2002) Displacement and nonlinear chromatographic techniques in the investigation of interaction of noncompetitive inhibitors with an immobilized $\alpha3\beta4$ nicotinic acetylcholine receptor liquid chromatographic stationary phase. *Anal. Chem. 74*, 4618–4624.

39. Jozwiak, K., Ravichandran, S., Collins, J. R., Moaddel, R., and Wainer, I. W. (2007) Interaction of noncompetitive inhibitors with the $\alpha3\beta2$ nicotinic acetylcholine receptor investigated by affinity chromatography and molecular docking. *J. Med. Chem. 50*, 6279–6283.

40. Spitzmaul, G., Dilger, J. P., and Bouzat, C. (2001) The noncompetitive inhibitor quinacrine modifies the desensitization kinetics of muscle acetylcholine receptors. *Mol. Pharmacol. 60*, 235–243.

41. Papke, R. L., and Oswald, R. E. (1989) Mechanisms of noncompetitive inhibition of acetylcholine-induced single-channel currents. *J. Gen. Physiol. 93*, 785–811.

42. Choi, J.-S., Choi, B. H., Ahn, H. S., Kim, M.-J., Rhie, D.-J., Yoon, S. H., Min, D. S., Jo, Y.-H., Kim, M.-S., Sung, K.-W., and Hahn S. J. (2003) Mechanism of block by fluoxetine of 5-hydroxytryptamine3 (5-HT$_3$)-mediated currents in NCB-20 neuroblastoma cells. *Biochem. Pharmacol. 66*, 2125–2132.

43. Pratt, M. B., Pedersen, S. E., and Cohen, J. B. (2000) Identification of the sites of incorporation of [^{3}H]ethidium diazide within the *Torpedo* nicotinic acetylcholine receptor ion channel. *Biochemistry 39*, 11452–11462.

44. Hamouda, A. K., Chiara, D. C., Blanton, M. P., and Cohen, J. B. (2008) Probing the structure of the affinity-purified and lipid-reconstituted *Torpedo* nicotinic acetylcholine receptor. *Biochemistry 47*, 12787–12794.

45. Eaton, M. J., Labarca, C., and Eterović, V. A. (2000) M2 mutations of the nicotinic acetylcholine receptor increase the potency of the non-competitive inhibitor phencyclidine. *J. Neurosci. Res. 61* 44–51.

46. Damaj, M. I., Carroll, F. I., Eaton, J. B., Navarro, H. A., Blough, B. E., Mirza, S., Lukas, R. J., and Martin, B. R. (2004) Enantioselective effects of hydroxyl metabolites of bupropion on behavior and on function of monoamine transporters and nicotinic receptors. *Mol. Pharmacol. 66*, 675–682.